PTEP

Prog. Theor. Exp. Phys. **2021**, 103D03 (23 pages)
DOI: 10.1093/ptep/ptab069

Electron wave functions in beta-decay formulas revisited (I): Gamow–Teller and spin-dipole contributions to allowed and first-forbidden transitions

Wataru Horiuchi[1], Toru Sato[2,3,*], Yuichi Uesaka[4], and Kenichi Yoshida[5]

[1]*Department of Physics, Hokkaido University, Sapporo 060-0810, Japan*
[2]*Research Center for Nuclear Physics, Osaka University, Ibaraki, Osaka 567-0047, Japan*
[3]*J-PARC Branch, KEK Theory Center, Institute of Particle and Nuclear Studies (KEK) and Theory Group, Particle and Nuclear Physics Division, J-PARC Center, Tokai, Ibaraki, 319-1106, Japan*
[4]*Faculty of Science and Engineering, Kyushu Sangyo University, Fukuoka 813-8503, Japan*
[5]*Department of Physics, Kyoto University, Kyoto 606-8502, Japan*
[*]E-mail: tsato@rcnp.osaka-u.ac.jp

Received April 1, 2021; Accepted May 18, 2021; Published June 4, 2021

We propose formulas of the nuclear beta-decay rate that are useful in a practical calculation. The decay rate is determined by the product of the lepton and hadron current densities. A widely used formula relies upon the fact that the low-energy lepton wave functions in a nucleus can be well approximated by a constant and are linear to the radius for the *s*-wave and *p*-wave wave functions, respectively. We find, however, that the deviation from such a simple approximation is evident for heavy nuclei with large Z by numerically solving the Dirac equation. In our proposed formulas, the neutrino wave function is treated exactly as a plane wave, while the electron wave function is obtained by iteratively solving the integral equation, thus we can control the uncertainty of the approximate wave function. The leading-order approximation gives a formula equivalent to the conventional one and overestimates the decay rate. We demonstrate that the next-to-leading-order formula reproduces well the exact result for a schematic transition density as well as a microscopic one obtained by a nuclear energy-density functional method.

Subject Index D02, D29

1. Introduction

The physics of exotic nuclei away from the stability line has been a major subject in nuclear physics. The lifetime of neutron-rich nuclei is governed by beta decay. Since the beta decay determines the time scale of the rapid-neutron-capture process (*r*-process) and the production of heavy elements together with the beta-delayed neutron(s) emission, the beta-decay rates of exotic nuclei are an important microscopic input for the simulation of nucleosynthesis [1]. The multi-messenger observations from a binary neutron star merger [2,3] imply that heavy neutron-rich nuclei that are even close to the drip line are involved in the *r*-process. Thus, the Coulomb effect on the beta particle (emitted electron) should be carefully examined under the extreme environment where the Q value for the beta decay, Q_β, is high and the nuclear charge Z is large.

A careful analysis of the Coulomb effect is also useful for a precision test of the standard model to find a signal of new physics by the search of deviation from the standard model. For example,

the effect on spectra of the beta particle and angular correlation as well as beta-decay rates has been studied to test the unitarity of the Cabibbo–Kobayashi–Maskawa (CKM) matrix, the scalar and tensor interactions, and the effect of neutrino mass in the allowed and first-forbidden transitions [4–7].

The formulation of nuclear beta decay within the distorted-wave impulse approximation of the electron Coulomb interaction has been developed [8–15]. The crucial part is how to handle the electron Coulomb wave function with a potential of the finite-size nuclear-charge distribution. Using the Maclaurin expansion of the nuclear radius r, the exact electron wave function was included in Ref. [16]. An iterative solution of the integral equation was found to have a better convergence by Behrens and Bühling [10,17]. The formula is arranged in the order of $\mathcal{O}(r^a V_C^b E_e^c m_e^d)$, where V_C, E_e and m_e represent the Coulomb potential, the energy and the mass of an electron, respectively. It has been widely used in the calculations such as in Refs. [18–20] and in the recent application to the r-process nuclei [21–32]. In most of those works, however, the leading-order approximation of the formula in Refs. [10,12] is adopted. Instead of expanding the lepton wave functions, one can incorporate the numerical solution of the charged lepton wave functions thanks to the advance of the computational ability. The muon capture [33] and the beta decay [15] are formulated suitably for this purpose. In this formulation, the nuclear matrix element is defined in a transparent way and appears similarly in Refs. [34,35] for the semi-leptonic nuclear processes and electron scattering [36]. It is thus straightforward to apply it to the charged-current neutrino reaction and lepton capture reaction. Developing an analytic formula of beta decay based on Ref. [15] would also contribute to a precise understanding of the neutrino–nucleus reactions to extract neutrino properties from neutrino experiments as discussed in Ref. [37,38].

The high-energy forbidden transitions occur under the exotic environment with high Q_β [39]. Therefore, in this work we revisit the formulation of beta decay for not only the allowed but also the first-forbidden transitions induced by the Gamow–Teller and spin-dipole type operators. We provide a simple way to improve the widely used formula in the nuclear beta-decay study to apply it to nuclei with large Z and away from the stability line. We start from the formulation of Koshigiri et al. [15] and use iterative solutions of the integral equation [10,17]. In the previous formalism, one often expands the electron and neutrino wave functions in the long-wavelength approximation and collect terms in a systematic way. Here we avoid this expansion of the neutrino wave function. We use an analytic form of the leading order (LO) and next-to-leading order (NLO) electron wave functions combined with the numerical table of the electron wave function at the origin. This makes the formula of the beta-decay rate simple and easy to use.

This paper is organized in the following way. We start from the formulation of the beta decay with the partial wave expansion for the lepton wave functions in Sect. 2. We provide an explicit expression of the first (LO) and the second (NLO) iteration of the integral equation for an electron wave function in Sect. 3. Formulas of the beta-decay rate are given and compared with the widely used one in Sect. 4. The formulas of LO and NLO are examined in Sect. 5, using a schematic transition density that is given by a sum of two Gaussians. We then in Sect. 6 apply the formulas to the neutron-rich Ni and Sn isotopes where the transition densities are microscopically obtained by a nuclear energy-density functional method. The summary and perspectives are given finally in Sect. 7.

2. Formalism

2.1. Effective Hamiltonian

An effective Hamiltonian for a low-energy charged-current reaction is given as

$$H_{\rm eff} = \frac{G_F V_{ud}}{\sqrt{2}} \int d\boldsymbol{x} [\bar{\ell}(\boldsymbol{x})\gamma^\mu(1-\gamma_5)\nu_\ell(\boldsymbol{x})J_\mu(\boldsymbol{x}) + \bar{\nu}_\ell(\boldsymbol{x})\gamma^\mu(1-\gamma_5)\ell(\boldsymbol{x})J^\dagger_\mu(\boldsymbol{x})], \tag{1}$$

where $\ell(\boldsymbol{x})$ represents either the electron, muon, or tau field, and $\bar{\psi} = \psi^\dagger\gamma^0$. The hadron current $J^\mu(\boldsymbol{x})$ is given by the vector and axial vector currents

$$J^\mu(\boldsymbol{x}) = V^\mu(\boldsymbol{x}) - A^\mu(\boldsymbol{x}), \tag{2}$$

where $G_{\rm F} = 1.166 \times 10^{-5}$ GeV^{-2} is the Fermi coupling constant and $V_{ud} = 0.9737$ is the CKM matrix [40]. Here we take natural units $\hbar = c = 1$.

The effective Hamiltonian describes semi-leptonic nuclear weak processes such as lepton capture, neutrino reaction, and $\beta^\pm$ decay. For β^- decay, $i \to e^-(p_e) + \bar{\nu}_e(p_\nu) + f$, where i and f respectively denote the initial and final nuclear states, and p_ℓ is the lepton momentum, the transition matrix element is given as

$$\left\langle e^-(p_e)\bar{\nu}_e(p_\nu)f \middle| H_{\rm eff} \middle| i \right\rangle = \frac{G_F V_{ud}}{\sqrt{2}} \int d\boldsymbol{x} \bar{\psi}^{(-)}_{e^-,p_e,s_e}(\boldsymbol{x})\gamma^\mu(1-\gamma_5)\nu_{s_\nu}(\boldsymbol{p}_\nu)e^{-i\boldsymbol{p}_\nu\cdot\boldsymbol{x}} \langle f| J_\mu(\boldsymbol{x}) |i\rangle , \tag{3}$$

and for β^+ decay,

$$\left\langle e^+(p_e)\nu_e(p_\nu)f \middle| H_{\rm eff} \middle| i \right\rangle = \frac{G_F V_{ud}}{\sqrt{2}} \int d\boldsymbol{x} \bar{u}_{s_\nu}(\boldsymbol{p}_\nu)e^{-i\boldsymbol{p}_\nu\cdot\boldsymbol{x}}\gamma^\mu(1-\gamma_5)\psi^{(+)}_{e^+,p_e,s_e}(\boldsymbol{x}) \langle f| J^\dagger_\mu(\boldsymbol{x}) |i\rangle , \tag{4}$$

where u and v are the Dirac spinors of the neutrino and anti-neutrino, respectively. The electron scattering wave functions ψ with the superscripts $(-)$ and $(+)$ satisfy the incoming and outgoing boundary conditions, respectively.

2.2. *Multipole expansion of the effective Hamiltonian*

The standard formulation of the beta decay adopts the partial wave expansion of both neutrino and electron wave functions. We use the following electron (charged lepton in general) scattering wave function

$$\psi^{(\mp)}_{e,p_e,s_e}(\boldsymbol{x}) = \sum_{\kappa_e,m_e,\mu_e} (4\pi) i^{l_{\kappa_e}} (l_{\kappa_e}, m_e, 1/2, s_e | j_{\kappa_e}, \mu_e) Y^*_{l_{\kappa_e},m_e}(\hat{p}_e) e^{\mp i\Delta_{\kappa_e}} \begin{pmatrix} G_{\kappa_e}(r)\chi^{\mu_e}_{\kappa_e} \\ iF_{\kappa_e}(r)\chi^{\mu_e}_{-\kappa_e} \end{pmatrix}. \tag{5}$$

Here, $(j_1, m_1, j_2, m_2|J, M)$ is the Clebsch–Gordan coefficient [41–43]. For positrons, G_{κ_e} and F_{κ_e} are calculated by replacing Z of the Coulomb interaction by $-Z$. Δ_{κ_e} is the Coulomb phase. The normalization of the scattering wave function in the plane wave expansion $\psi_e(\boldsymbol{x}) \to u(p_e)\exp(i\boldsymbol{p}_e\cdot\boldsymbol{x})$ is given as

$$u_{s_e}(p_e) = \sqrt{\frac{E_e + m_e}{2E_e}} \begin{pmatrix} 1 \\ \frac{\boldsymbol{\sigma}\cdot\boldsymbol{p}_e}{E_e+m_e} \end{pmatrix} \chi_{s_e}. \tag{6}$$

It is noticed that the electron wave functions (G_κ, F_κ) in Ref. [15] are defined by multiplying $e^{i\Delta_{\kappa_e}}$ with our (G_κ, F_κ), while those of Refs. [10,16] are given by multiplying $\sqrt{2}p_e$ with ours.

The neutrino and anti-neutrino wave functions are respectively expanded as

$$u_{s_\nu}(\boldsymbol{p}_\nu)e^{i\boldsymbol{p}_\nu\cdot\boldsymbol{r}} = \sum_{\kappa_\nu,m_\nu,\mu_\nu} \frac{4\pi}{\sqrt{2}} i^{l_{\kappa_\nu}} Y^*_{l_{\kappa_\nu}m_\nu}(\hat{p}_\nu)(l_{\kappa_\nu},m_\nu,1/2,s_\nu|j_{\kappa_\nu},\mu_\nu) \begin{pmatrix} g_{\kappa_\nu}(r)\chi^{\mu_\nu}_{\kappa_\nu} \\ if_{\kappa_\nu}(r)\chi^{\mu_\nu}_{-\kappa_\nu} \end{pmatrix}, \tag{7}$$

$$v_{s_\nu}(\boldsymbol{p}_\nu)e^{-i\boldsymbol{p}_\nu\cdot\boldsymbol{r}} = \sum_{\kappa_\nu,m_\nu,\mu_\nu} \frac{4\pi}{\sqrt{2}} i^{-l_{\kappa_\nu}} Y^*_{l_{\kappa_\nu}m_\nu}(\hat{p}_\nu)(l_{\kappa_\nu},m_\nu,1/2,-s_\nu|j_{\kappa_\nu},\mu_\nu)(-1)^{1/2-s_\nu} \times \begin{pmatrix} -if_{\kappa_\nu}(r)\chi^{\mu_\nu}_{-\kappa_\nu} \\ g_{\kappa_\nu}(r)\chi^{\mu_\nu}_{\kappa_\nu} \end{pmatrix}, \tag{8}$$

with

$$g_\kappa(r) = j_{l_\kappa}(p_\nu r), \tag{9}$$

$$f_\kappa(r) = S_\kappa j_{\bar{l}_\kappa}(p_\nu r), \tag{10}$$

where $j_l(x)$ is the spherical Bessel function of order l, $S_\kappa = \mathrm{sgn}(\kappa)$ is the sign of κ, and $\bar{l}_\kappa = l_{-\kappa}$.

With the partial wave expansion of the electron and neutrino wave functions, one obtains the following form [15]:

$$H_{\rm eff} = \frac{G_F V_{ud}}{\sqrt{2}} \sqrt{\frac{(4\pi)^3}{2}} \sum_{el}\sum_{neu}\sum_{L,J} (j_e,-\mu_e,j_\nu,\mu_\nu|J,M)(-1)^{1/2-\mu_e}\,\Xi_{JLM}(\kappa_e,\kappa_\nu), \tag{11}$$

and

$$\begin{aligned}\Xi_{JLM}(\kappa_e,\kappa_\nu) = S_{\kappa_e}\int d\boldsymbol{r} \\ &\times \Big\{ \mp Y_{JM}(\hat{r})V_0(\boldsymbol{r})\delta_{L,J}(G_{\kappa_e}(r)g_{\kappa_\nu}(r)S_{0JJ}(\kappa_e,\kappa_\nu) + F_{\kappa_e}(r)f_{\kappa_\nu}(r)S_{0JJ}(-\kappa_e,-\kappa_\nu)) \\ &\pm i[Y_L(\hat{r})\otimes \boldsymbol{V}(\boldsymbol{r})]_{JM}(G_{\kappa_e}(r)f_{\kappa_\nu}(r)S_{1LJ}(\kappa_e,-\kappa_\nu) - F_{\kappa_e}(r)g_{\kappa_\nu}(r)S_{1LJ}(-\kappa_e,\kappa_\nu)) \\ &+ iY_{JM}(\hat{r})A_0(\boldsymbol{r})\delta_{L,J}(G_{\kappa_e}(r)f_{\kappa_\nu}(r)S_{0JJ}(\kappa_e,-\kappa_\nu) - F_{\kappa_e}(r)g_{\kappa_\nu}(r)S_{0JJ}(-\kappa_e,\kappa_\nu)) \\ &- [Y_L(\hat{r})\otimes \boldsymbol{A}(\boldsymbol{r})]_{JM}(G_{\kappa_e}(r)g_{\kappa_\nu}(r)S_{1LJ}(\kappa_e,\kappa_\nu) + F_{\kappa_e}(r)f_{\kappa_\nu}(r)S_{1LJ}(-\kappa_e,-\kappa_\nu))\Big\},\end{aligned} \tag{12}$$

where $[\mathcal{O}_{k_1}\otimes\mathcal{O}'_{k_2}]_{k_3m_3}$ denotes the tensor product. Here we adopt the following simplified notation for $\sum_{el}$ and $\sum_{neu}$:

$$\sum_{el} = \sum_{\kappa_e,\mu_e} i^{-l_{\kappa_e}} e^{i\Delta_{\kappa_e}}(l_{\kappa_e},m_e,1/2,s_e|j_{\kappa_e},\mu_e)Y_{l_{\kappa_e}m_e}(\hat{p}_e), \tag{13}$$

$$\sum_{neu} = \sum_{\kappa_\nu,\mu_\nu} i^{-l_{\kappa_\nu}}(-1)^{1/2-s_\nu} \times [Y^*_{l_{\kappa_\nu}m_\nu}(\hat{p}_\nu)(l_{\kappa_\nu},m_\nu,1/2,-s_\nu|j_{\kappa_\nu},\mu_\nu) \pm Y^*_{\bar{l}_\kappa m_\nu}(\hat{p}_\nu)(\bar{l}_{\kappa_\nu},m_\nu,1/2,-s_\nu|j_{\kappa_\nu},\mu_\nu)], \tag{14}$$

and

$$S_{KLJ}(\kappa',\kappa) = \sqrt{2(2j_\kappa+1)(2j_{\kappa'}+1)(2l_\kappa+1)(2l_{\kappa'}+1)(2K+1)} \times (l_\kappa,0,l_{\kappa'},0|L,0) \begin{Bmatrix} l_{\kappa'} & 1/2 & j_{\kappa'} \\ l_\kappa & 1/2 & j_\kappa \\ L & K & J \end{Bmatrix}. \tag{15}$$

Using the above form of the effective Hamiltonian, the beta-decay rate is given by integrating the scattering angles of the neutrino and electron as

$$\Gamma = \frac{(G_F V_{ud})^2}{\pi^2} \int_{m_e}^{E_0} dE_e p_e E_e (E_0 - E_e)^2 \sum_{J,L,\kappa_e,\kappa_\nu} \frac{1}{2J_i+1} |\langle f \| \Xi_{JL}(\kappa_e,\kappa_\nu) \| i \rangle|^2, \tag{16}$$

where J_i is the angular momentum of the initial state. Neglecting the mass of a neutrino, the maximum energy of an electron E_0 is the Q value of the nuclear transition, Q_β. See Appendix A for the derivation.

3. Electron Coulomb wave function

3.1. *Parametrization of lepton wave function*

The general formula given in Eq. (12) is ready for the use of any allowed and forbidden transition rates by evaluating the nuclear transition density. However, an explicit formula for the allowed and first-forbidden transitions helps extract nuclear structure information from the beta-decay observables. Since the electron Coulomb wave function is rather involved in evaluating the beta-decay rate, we briefly describe the derivation of the expression of charged-lepton wave functions by iterating the integral equation following Refs. [10,17].

A Dirac wave function of an electron is given as

$$[\boldsymbol{\alpha} \cdot \boldsymbol{p}_e + \beta m_e + V_C(r)]\psi_e(\boldsymbol{r}) = E_e \psi_e(\boldsymbol{r}). \tag{17}$$

The electron wave functions G_κ, F_κ satisfy the coupled first-order differential equation with the Coulomb potential V_C:

$$\frac{dG_\kappa}{dr} + \frac{1+\kappa}{r} G_\kappa - (m_e + E_e - V_C) F_\kappa = 0, \tag{18}$$

$$\frac{dF_\kappa}{dr} + \frac{1-\kappa}{r} F_\kappa - (m_e - E_e + V_C) G_\kappa = 0. \tag{19}$$

Throughout this paper we keep the electron mass explicit so that in future we can use the formula for the muon neutrino reactions. Electron wave functions are parametrized by taking into account the behavior of the wave function at the origin $r \sim 0$ [10] as

$$G_{-k}(r) = \alpha_{-k} \frac{(p_e r)^{k-1}}{(2k-1)!!} [H_k(r) - h_k(r)], \tag{20}$$

$$F_k(r) = \alpha_k \frac{(p_e r)^{k-1}}{(2k-1)!!} [H_k(r) + h_k(r)], \tag{21}$$

$$G_k(r) = \alpha_k \frac{(p_e r)^{k-1}}{(2k-1)!!} \frac{r}{R} [D_k(r) + d_k(r)], \tag{22}$$

$$F_{-k}(r) = -\alpha_{-k} \frac{(p_e r)^{k-1}}{(2k-1)!!} \frac{r}{R} [D_k(r) - d_k(r)]. \tag{23}$$

Here $k > 0$ and $H_k(0) = 1$ and $h_k(0) = 0$. The normalization of the electron wave functions are determined by constants α_κ. This parametrization of G_κ, F_κ incorporates the boundary condition of

the wave function at the origin. Then the following set of coupled integral equations is obtained:

$$H_k(r) = 1 + \int_0^r \frac{r'}{R}[(-E_e + V_C(r'))D_k(r') + m_e d_k(r')]dr', \tag{24}$$

$$h_k(r) = \int_0^r \frac{r'}{R}[m_e D_k(r') + (-E_e + V_C(r'))d_k(r')]dr', \tag{25}$$

$$\frac{r}{R}D_k(r) = \int_0^r \left(\frac{r'}{r}\right)^{2k}[(E_e - V_C(r'))H_k(r') + m_e h_k(r')]dr', \tag{26}$$

$$\frac{r}{R}d_k(r) = \int_0^r \left(\frac{r'}{r}\right)^{2k}[m_e H_k(r') + (E_e - V_C(r'))h_k(r')]dr'. \tag{27}$$

At this stage R is just a parameter of dimension length. We take R as the nuclear radius though the final formulas are independent of the choice of R.

3.2. Iterative solution of integral equation

Taking into account the boundary condition, H_k, h_k, D_k, and d_k are expanded according to the number of iteration as

$$H_k(r) = 1 + H_k^{(2)}(r) + H_k^{(4)}(r) + \cdots, \tag{28}$$

$$h_k(r) = h_k^{(2)}(r) + h_k^{(4)}(r) + \cdots, \tag{29}$$

$$D_k(r) = D_k^{(1)}(r) + D_k^{(3)}(r) + \cdots, \tag{30}$$

$$d_k(r) = d_k^{(1)}(r) + d_k^{(3)}(r) + \cdots. \tag{31}$$

The first iteration of the integral equation gives

$$\frac{r}{R}D_k^{(1)}(r) = \int_0^r \left(\frac{r'}{r}\right)^{2k}(E_e - V_C(r'))dr', \tag{32}$$

$$\frac{r}{R}d_k^{(1)}(r) = \int_0^r \left(\frac{r'}{r}\right)^{2k} m_e dr', \tag{33}$$

and further iterations give

$$H_k^{(2n)}(r) = \int_0^r \left[(-E_e + V_C(r'))\frac{r'}{R}D_k^{(2n-1)}(r') + m_e\frac{r'}{R}d_k^{(2n-1)}(r')\right]dr', \tag{34}$$

$$h_k^{(2n)}(r) = \int_0^r \left[m_e\frac{r'}{R}D_k^{(2n-1)}(r') + (-E_e + V_C(r'))\frac{r'}{R}d_k^{(2n-1)}(r')\right]dr', \tag{35}$$

and

$$\frac{r}{R}D_k^{(2n+1)}(r) = \int_0^r \left(\frac{r'}{r}\right)^{2k}\left[(E_e - V_C(r'))H_k^{(2n)}(r') + m_e h_k^{(2n)}(r')\right]dr', \tag{36}$$

$$\frac{r}{R}d_k^{(2n+1)}(r) = \int_0^r \left(\frac{r'}{r}\right)^{2k}\left[m_e H_k^{(2n)}(r') + (E_e - V_C(r'))h_k^{(2n)}(r')\right]dr', \tag{37}$$

for $n = 1, 2, \ldots$. The exact electron wave functions in terms of E_e, m_e, and V_C are obtained from the iterative solution of the above equations.

3.3. LO and NLO electron wave functions

We denote the leading order (LO) electron wave function as

$$H_k^{\rm LO}(r) = 1, \tag{38}$$

$$h_k^{\rm LO}(r) = 0, \tag{39}$$

$$\frac{r}{R}D_k^{\rm LO}(r) = \frac{r}{R}D_k^{(1)}(r) = \frac{E_e r}{2k+1} + V_{D1}(r), \tag{40}$$

$$\frac{r}{R}d_k^{\rm LO}(r) = \frac{r}{R}d_k^{(1)}(r) = \frac{m_e r}{2k+1}, \tag{41}$$

with

$$V_{D1}(r) = -\int_0^r \left(\frac{r'}{r}\right)^{2k} V_C(r')dr'. \tag{42}$$

Adding the next-to-leading order (NLO), the NLO wave function is given as

$$H_k^{\rm NLO}(r) = 1 + H_k^{(2)}(r), \tag{43}$$

$$h_k^{\rm NLO}(r) = h_k^{(2)}(r), \tag{44}$$

$$\frac{r}{R}D_k^{\rm NLO}(r) = \frac{r}{R}(D_k^{(1)}(r) + D_k^{(3)}(r)), \tag{45}$$

$$\frac{r}{R}d_k^{\rm NLO}(r) = \frac{r}{R}(d_k^{(1)}(r) + d_k^{(3)}(r)), \tag{46}$$

where

$$H_k^{(2)}(r) = -\frac{p_e^2 r^2}{2(2k+1)} + V_{H2}(r), \tag{47}$$

$$h_k^{(2)}(r) = V_{h2}(r), \tag{48}$$

$$\frac{r}{R}D_k^{(3)}(r) = -\frac{p_e^2 E_e r^3}{2(2k+1)(2k+3)} + V_{D3}(r), \tag{49}$$

$$\frac{r}{R}d_k^{(3)}(r) = -\frac{p_e^2 m_e r^3}{2(2k+1)(2k+3)} + V_{d3}(r), \tag{50}$$

with

$$V_{H2}(r) = \int_0^r \left[(V_C(r') - E_e)V_{D1}(r') + E_e\frac{r'}{2k+1}V_C(r')\right]dr', \tag{51}$$

$$V_{h2}(r) = m_e\int_0^r \left[V_{D1}(r') + \frac{r'}{2k+1}V_C(r')\right]dr', \tag{52}$$

$$V_{D3}(r) = \int_0^r \left(\frac{r'}{r}\right)^{2k}\left[(E_e - V_C(r'))V_{H2}(r') + m_e V_{h2}(r') + \frac{p_e^2 r'^2}{2(2k+1)}V_C(r')\right]dr', \tag{53}$$

$$V_{d3}(r) = \int_0^r \left(\frac{r'}{r}\right)^{2k}[m_e V_{H2}(r') + (E_e - V_C(r'))V_{h2}(r')]dr'. \tag{54}$$

The explicit expressions of $H_k^{(2)}, h_k^{(2)}, D_k^{(i)}$, and $d_k^{(i)}$ for the uniform charge distribution are given in Appendix B.

4. Decay rate and comparison with the conventional formula

4.1. Decay rate

The beta-decay rate is usually expressed in terms of the Fermi function $F(Z,E_e)$ and the shape correction factor $C(E_e)$ as [12,14]

$$\Gamma = \frac{(G_F V_{ud})^2}{2\pi^3}\int_{m_e}^{E_0} dE_e p_e E_e (E_0 - E_e)^2 F(Z,E_e) C(E_e). \tag{55}$$

Using the matrix element of the effective operator Ξ_{JLM}, we obtain

$$F(Z,E_e)C(E_e) = \sum_{J,L,\kappa_e,\kappa_\nu} \frac{2\pi}{2J_i+1} |\,\langle f \|\, \Xi_{JL}(\kappa_e,\kappa_\nu)\,\| i\rangle\,|^2, \tag{56}$$

and $F(Z,E_e) = \alpha_{-1}^2 + \alpha_1^2$.

4.2. Allowed and first-forbidden transitions of axial vector current

We focus on the transition rate due to the space component of the axial vector current. In the impulse approximation, the axial vector current is given as

$$\boldsymbol{A}(\boldsymbol{r}) = g_A \sum_{\tau,\tau'}\sum_{\sigma,\sigma'} \psi^\dagger(\boldsymbol{r}\sigma\tau)\psi(\boldsymbol{r}\sigma'\tau')\langle\tau|\tau^\mp|\tau'\rangle\langle\sigma|\boldsymbol{\sigma}|\sigma'\rangle, \tag{57}$$

with the nucleon field operators $\psi, \psi^\dagger$ at position $\boldsymbol{r}$, spin σ, and isospin τ. The transition density $\rho_{JL}(r)$ represented in the radial coordinate is defined as

$$g_{\rm A}\rho_{JL}(r) = \langle f \|\, \int d\Omega_r [Y_L(\hat{r}) \otimes \boldsymbol{A}(\boldsymbol{r})]_J \,\| i\rangle\,. \tag{58}$$

The reduced matrix element of the effective operator Ξ_{JLM} is given in terms of the radial integral of the transition density $\rho_{JL}(r)$ multiplied by combination of the electron and neutrino wave functions with the coefficients c_g and c_f given in Appendix C:

$$\begin{aligned}\langle f \|\, \Xi_{JL}(\kappa_e,\kappa_\nu)\,\| i\rangle &= \langle f \|\, \int d\boldsymbol{r} [Y_L(\hat{r}) \otimes \boldsymbol{A}(\boldsymbol{r})]_J [c_g G_{\kappa_e}(r) g_{\kappa_\nu}(r) + c_f F_{\kappa_e}(r) f_{\kappa_\nu}(r)]\,\| i\rangle \\ &= g_{\rm A}\int_0^\infty dr r^2 \rho_{JL}(r)[c_g G_{\kappa_e}(r) g_{\kappa_\nu}(r) + c_f F_{\kappa_e}(r) f_{\kappa_\nu}(r)].\end{aligned} \tag{59}$$

The leading-order formula by Behrens–Bühring (LOB) of Ref. [10] conventionally used in the nuclear structure calculations can be derived by using approximate lepton wave functions in Eqs. (56) and (59). We take the LO electron wave function and the leading-order approximation of the neutrino wave function. For the allowed transition with $\Delta J^\pi = 1^+$, we approximate the s-wave wave functions as a constant number:

$$G_{-1}(r) \sim \alpha_{-1}, \quad g_{-1}(r) \sim 1, \tag{60}$$

$$F_1(r) \sim \alpha_1, \quad f_1(r) \sim 1, \tag{61}$$

and neglect all other partial waves. For the spin-dipole transition with $\Delta J^\pi = 0^-, 1^-$, and 2^-, in addition to the above approximation to the s-wave wave function, we use the following leading-order

approximation for the p-wave wave functions:

$$G_1(r) \sim \alpha_1 \frac{r}{3}[E_e + m_e + \frac{3V_{D1}(r)}{r}], \quad g_1(r) \sim \frac{p_\nu r}{3}, \tag{62}$$

$$F_{-1}(r) \sim -\alpha_{-1} \frac{r}{3}[E_e - m_e + \frac{3V_{D1}(r)}{r}], \quad f_{-1}(r) \sim -\frac{p_\nu r}{3}, \tag{63}$$

$$G_{-2}(r) \sim \alpha_{-2} \frac{p_e r}{3}, \quad g_{-2}(r) \sim \frac{p_\nu r}{3}, \tag{64}$$

$$F_2(r) \sim \alpha_2 \frac{p_e r}{3}, \quad f_2(r) \sim \frac{p_\nu r}{3}. \tag{65}$$

For the allowed $\Delta J^\pi = 1^+$ transition, two partial waves of leptons $(\kappa_e, \kappa_\nu) = (-1, -1)$ and $(1, 1)$ contribute within LOB:

$$\sum_{\kappa_e,\kappa_\nu} \left| \langle f \| \, \Xi_{J=1,L=0} \, \| i \rangle \right|^2 \sim 2g_{\rm A}^2 \left\{ \left| \int_0^\infty dr r^2 \rho_{10}(r) \left[G_{-1}(r) g_{-1}(r) + \frac{1}{3} F_{-1}(r) f_{-1}(r) \right] \right|^2 \right.$$
$$\left. + \left| \int_0^\infty dr r^2 \rho_{10}(r) \left[\frac{1}{3} G_1(r) g_1(r) + F_1(r) f_1(r) \right] \right|^2 \right\} \tag{66}$$

$$\sim 2g_{\rm A}^2 (\alpha_{-1}^2 + \alpha_1^2) \left| \int_0^\infty dr r^2 \rho_{10}(r) \right|^2. \tag{67}$$

In the last step, we use the approximation for the lepton wave functions. As a result the shape correction factor is given as

$$C(E_e) = g_{\rm A}^2 \left| \int_0^\infty dr r^2 \sqrt{4\pi} \rho_{10}(r) \right|^2. \tag{68}$$

The second example is the first-forbidden transition $\Delta J^\pi = 0^-$. The leading-order partial waves are $(\kappa_e, \kappa_\nu) = (-1, 1)$ and $(1, -1)$. We then obtain

$$\sum_{\kappa_e,\kappa_\nu} | \, \langle f \| \, \Xi_{J=0,L=1} \, \| i \rangle \, |^2 \sim 2g_{\rm A}^2 \left\{ \left| \int_0^\infty dr r^2 \rho_{01}(r) [G_{-1}(r) g_1(r) - F_{-1}(r) f_1(r)] \right|^2 \right.$$
$$\left. + \left| \int_0^\infty dr r^2 \rho_{01}(r) [G_1(r) g_{-1}(r) - F_1(r) f_{-1}(r)] \right|^2 \right\} \tag{69}$$

$$\sim \frac{2}{9} g_{\rm A}^2 \left\{ \alpha_{-1}^2 \left| \int_0^\infty dr r^3 \rho_{01}(r) \left[p_\nu + E_e - m_e + 3 \frac{V_{D1}(r)}{r} \right] \right|^2 \right.$$
$$\left. + \alpha_1^2 \left| \int_0^\infty dr r^3 \rho_{01}(r) \left[p_\nu + E_e + m_e + 3 \frac{V_{D1}(r)}{r} \right] \right|^2 \right\}. \tag{70}$$

In order to compare our formula with LOB, e.g. Eq. (10.56) of Ref. [11], introducing nuclear matrix elements

$$\omega = g_{\rm A} \sqrt{4\pi} \int_0^\infty dr r^3 \rho_{01}(r), \tag{71}$$

$$\xi \omega' = g_{\rm A} \sqrt{4\pi} \int_0^\infty dr r^2 \rho_{01}(r) V_{D1}(r), \tag{72}$$

we obtain

$$C(E_e) = \zeta_0^2 + \frac{\omega^2 m_e^2}{9} - \frac{2}{3}\frac{\mu_1\gamma_1 m_e^2}{E_e}\zeta_0\omega, \tag{73}$$

where

$$\zeta_0 = \frac{E_e\omega}{3} + \xi\omega', \tag{74}$$

$$\gamma_k = \sqrt{k^2 - (\alpha Z)^2}, \tag{75}$$

$$\mu_k = \frac{k}{\gamma_k}\frac{E_e}{m_e}\frac{\alpha_{-k}^2 - \alpha_k^2}{\alpha_{-1}^2 + \alpha_1^2}. \tag{76}$$

Here α is the fine structure constant. A similar comparison can be done for the transitions to 1^- and 2^- states, and we can confirm that the use of the approximate lepton wave function within our formalism leads to the "conventional" formula of the decay rate.

5. Analysis with a schematic model

In the following, we examine the validity of the approximation for the electron wave function proposed in this work by using a schematic model of transition density. Three sets of treatment of the lepton wave function, (i) exact, (ii) LO, and (iii) NLO, are defined. By (i) "exact", we use the electron wave function obtained by a numerical solution of the Dirac equation and the spherical Bessel function for the neutrino wave function. In (ii) LO and (iii) NLO, we approximate the electron wave function by the LO and NLO wave functions described in the previous section. Notice that we do not expand the neutrino wave function. We use the uniform charge distribution for the nuclear charge with a charge radius $R_A = 1.2 \times A^{1/3}$ fm, and a transition density given by a sum of two Gaussians. The analytic expressions for the LO and NLO terms of the electron wave functions are summarized in Appendix B. We found that the numerical results of LO are very close to those of the "conventional" formula LOB.

The explicit forms of the LO and NLO approximation of the electron wave functions of $\kappa_e = -1$ with the s-wave large component (G_{-1}) and the p-wave small component (F_{-1}) are given as

$$G_{-1}^{\rm LO}(r) = \alpha_{-1}, \tag{77}$$

$$F_{-1}^{\rm LO}(r) = -\alpha_{-1} r\left[\frac{E_e - m_e}{3} + \xi s_1(x)\right], \tag{78}$$

$$G_{-1}^{\rm NLO}(r) = G_{-1}^{\rm LO}(r) + \alpha_{-1} r^2\left[-\frac{p_e^2}{6} + \xi(E_e s_2(x) - m_e h_2(x)) + \xi^2 t_2(x)\right], \tag{79}$$

$$\begin{aligned} F_{-1}^{\rm NLO}(r) =& F_{-1}^{\rm LO}(r) - \alpha_{-1} r^3\left[-\frac{p_e^2(E_e - m_e)}{30} + \xi(p_e^2 s_3(x) + m_e(m_e - E_e)t_3(x))\right. \\ &\left. + \xi^2(E_e w_3(x) - m_e z_3(x)) + \xi^3 y_3(x)\right], \end{aligned} \tag{80}$$

where $x = r/R_A$ and $\xi = \alpha Z/(2R_A)$.

Figure 1 shows the electron wave functions G_{-1} and F_{-1} at $E_e = 10$ MeV for $Z = 82$ and $A = 208$. The "exact" and "LO" wave functions are shown by the solid and short-dashed curves, respectively. The deviation of the LO wave function from the exact one grows as r increases. One can see that the deviation is larger for an s-wave than a p-wave wave function. By taking into account

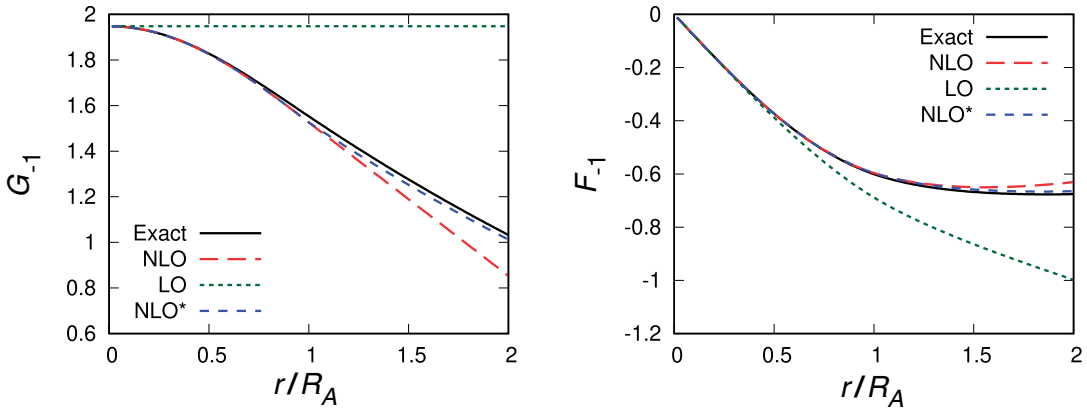

Fig. 1. Electron wave functions G_{-1} (left) and F_{-1} (right) for $Z = 82, A = 208, \kappa_e = -1$ and $E_e = 10$ MeV. The NLO wave function of this work and the LO wave function approximately corresponding to "conventional" (LOB) are compared. NLO* denotes that obtained by connecting the NLO wave function with the point Coulomb regular and irregular wave functions at $r = R_A$.

the NLO correction, the wave functions are greatly improved, but a slight deviation from the "exact" wave function still remains for a larger r region. For the uniform charge distribution, the Coulomb potential for $r > R_A$ agrees with the point Coulomb potential. Therefore, by connecting the NLO wave function with the combination of the analytic form of the regular and irregular point Coulomb wave functions, we can obtain the electron wave functions for $r > R_A$ with improved accuracy (NLO*). This is indeed the case, as shown in the blue dashed curves in Fig. 1. Figure 2 is the same as Fig. 1 but for $Z = 28, A = 80$. One sees that the effects of the NLO correction are smaller than in the $Z = 82$ case, though the deviation of the LO wave function is distinct for the s-wave.

For β^+ decay, the sign changes for the odd power terms of ξ. The Coulomb potential enters in the Dirac equation in the form of $E_e - V_C$ as given in Eqs. (18) and (19). The Coulomb effect is constructive to E_e for an electron, while it is destructive for a positron. For $E_e > |V_C|$, the deviation from the LO wave function becomes smaller for a positron than for an electron.

The E_e and Z dependence of the NLO correction is parametrized essentially by two non-dimensional parameters, $R_A E_e$ and $R_A \xi = \alpha Z/2$. Figure 3 shows the deviation of the approximate LO and NLO electron wave functions G_{-1} at the nuclear surface $r = R_A$, $[G_{-1}(\text{approx.})/G_{-1}(\text{exact}) - 1] \times 100$, as a function of $R_A E_e$ and Z. One sees a considerable deviation for a larger nuclear charge Z and a higher $R_A E_e$ value. The LO approximation overestimates the amplitude of the wave function at the nuclear surface. By including the NLO correction, the error is notably reduced. For $E_e = 10$ MeV, the case of $Z = 82, A = 208$ and $Z = 28, A = 80$ corresponds to $R_A E_e \sim 0.30, R_A \xi \sim 0.36$ and $R_A E_e \sim 0.26, R_A \xi \sim 0.10$, respectively.

The difference between the LO and "exact" lepton wave functions observed above certainly affects the beta-decay rate. The magnitude of the effect depends on the transition density of nuclear weak currents. To examine the effects on the beta-decay rate, we take the following simple form of the transition density for the Gamow–Teller and spin-dipole transitions:

$$\rho_{\rm tr} = \mathcal{N}\left[a\, e^{-(r-r_1)^2/b^2} + e^{-(r-r_2)^2/b^2}\right]. \tag{81}$$

Here we take $r_1 = 0.9R_A, b = R_A/4$ and $r_2 = 3r_1/4$. By varying $-1 \le a \le -0.2$, we investigate the validity of the approximation for the electron wave function on the decay rate. The transition

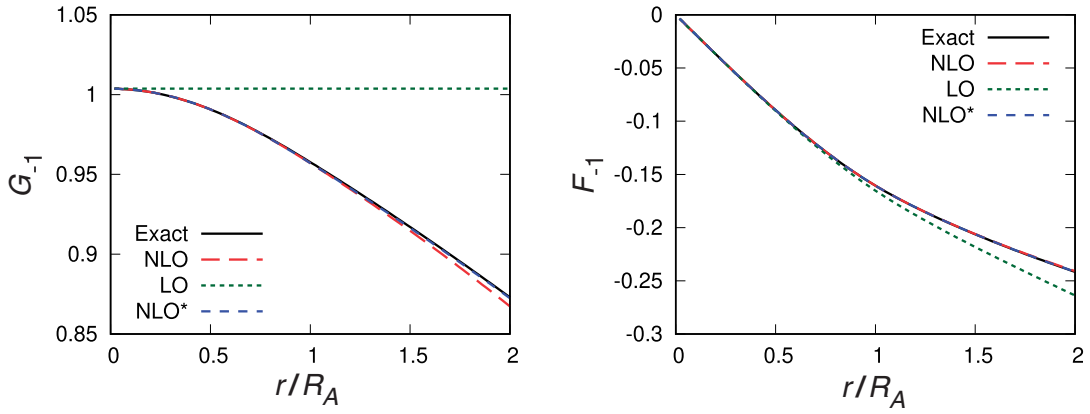

Fig. 2. Same as Fig. 1 but for $Z = 28$ and $A = 80$.

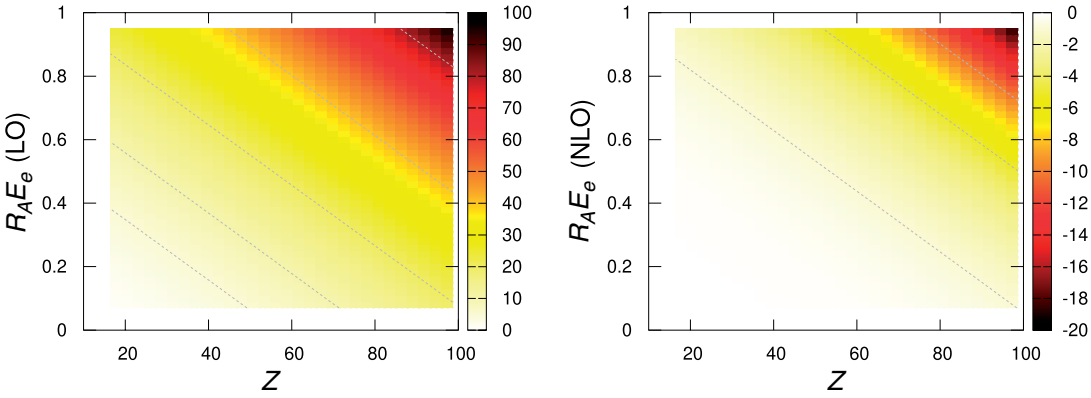

Fig. 3. Relative deviation $[G_{-1}(\text{approx.})/G_{-1}(\text{exact}) - 1] \times 100$ as a function of $R_A E_e$ and Z. The LO wave function (left) and NLO wave function (right) is used for the approximate electron wave function. As a guide, the position where the relative deviation is equal is indicated by the dotted curves.

density multiplied by r^2, $(r/R_A)^2 \rho_{\rm tr}(r)$, is shown in Fig. 4 with a as a parameter. For $a = -0.2$, the contribution of the $r < R_A$ region is predominant for the transition matrix element, while for $a = -1$, the $r \sim R_A$ region gives a prevailing contribution to the matrix element. For $a = -0.6$, a strong suppression of the matrix element would take place.

In what follows, we examine the validity of the LO and NLO approximations of the electron wave function. The decay rate is studied for $Z = 82$, $A = 208$ with $E_0 = 10$ MeV using the transition density (81). In Fig. 5, the decay rate evaluated using the "exact" electron wave function is shown by the solid curve with $\Delta a = 0.025$ in arbitrary unit normalized to unity at $a = -0.8$. The LO and NLO results are shown by the dashed and dotted curves, respectively. Strong suppression of the transition rate of the allowed Gamow–Teller transition is seen around $a = -0.6$, while it happens around $a = -0.5$ for the 0^- transition. For the first-forbidden transition, an extra factor r of the operator moves the minimum position of the matrix element slightly. The deviation of LO from the exact calculation is large for $a < -0.6$, where the contribution at $r \sim R_A$ is more important than at $r < R_A$. The suppression takes place at larger a for LO than the exact calculation. The use of the augmented NLO electron wave function significantly improves for $a < -0.7$, and works reasonably well even when a severe cancellation between the inner and the outer contribution of the integration

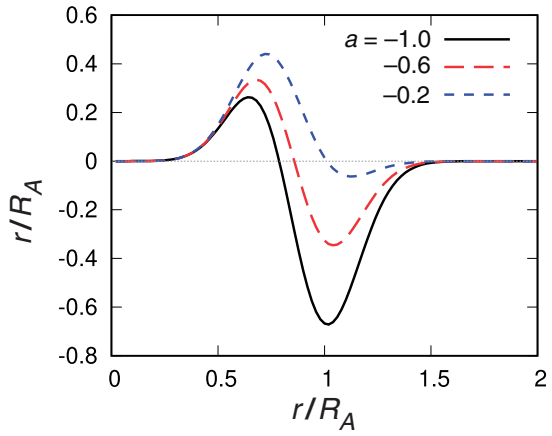

Fig. 4. Transition density used in the present simple model analysis multiplied by $(r/R_A)^2$ with $\mathcal{N} = 1$ as a function of the scaled radial coordinate r/R_A. See text for details. The dotted horizontal line indicates zero.

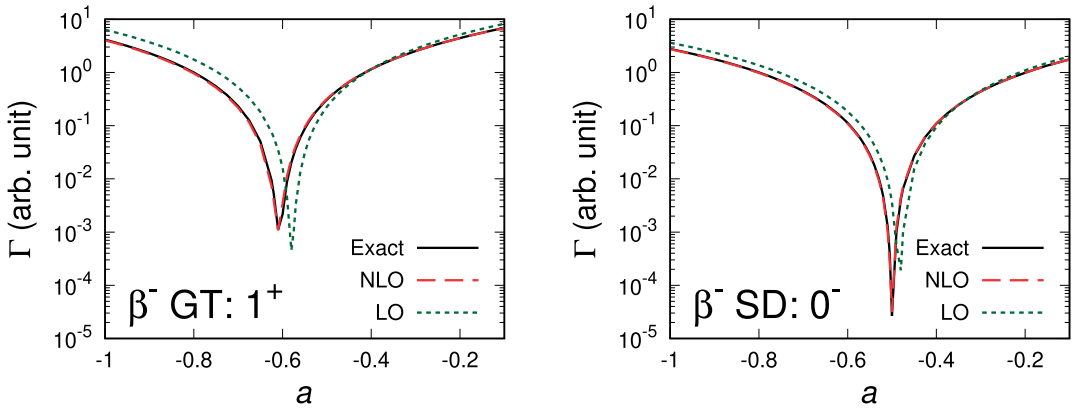

Fig. 5. a dependence of the decay rate for the Gamow–Teller (GT) $\Delta J^\pi = 1^+$ (left) and spin-dipole (SD) $\Delta J^\pi = 0^-$ (right) transitions of β^- decay. The beta decay rate of $Z = 82$, $A = 208$ and $E_0 = 10$ MeV is calculated using the "exact" wave function is shown by the solid (black) curve with $\Delta a = 0.025$ and is connected by the solid (black) lines. The rate is normalized as unity at $a = -0.8$. The decay rate using the NLO and the LO are shown by the dashed (red) and dotted (green) curves, respectively.

takes place around $a = -0.6$. We obtain a similar a dependence of the β^+ decay rate shown in Fig. 6. For β^+ decay, the LO approximation gives reasonable description for $Z = 82$ and $E_0 = 10$ MeV.

At the end of the study with the schematic model, we investigate the Z dependence of the NLO correction. Figure 7 shows the Z dependence of the β^- decay rate for $E_0 = 10$ MeV calculated by LO, $\Gamma(\text{LO})/\Gamma(\text{exact})$, and by NLO, $\Gamma(\text{NLO})/\Gamma(\text{exact})$, for the Gamow–Teller and spin-dipole transitions. Here the transition density with a moderate cancellation of the matrix element with $a = -0.8$ is used. One sees a simple use of the LO or conventional (LOB) formula overestimates the exact rate by about 50–100% for heavy nuclei. This significant overestimation is mainly due to the deviation of the s-wave electron wave function from constant value around the nuclear surface, as shown in Fig 1. This suggests that the transition probability extracted from the beta-decay rate using the LO can be underestimated for the transition involving heavy neutron-rich nuclei. However, it is apparent that our NLO approximation works well for a wide range of the nuclear charge.

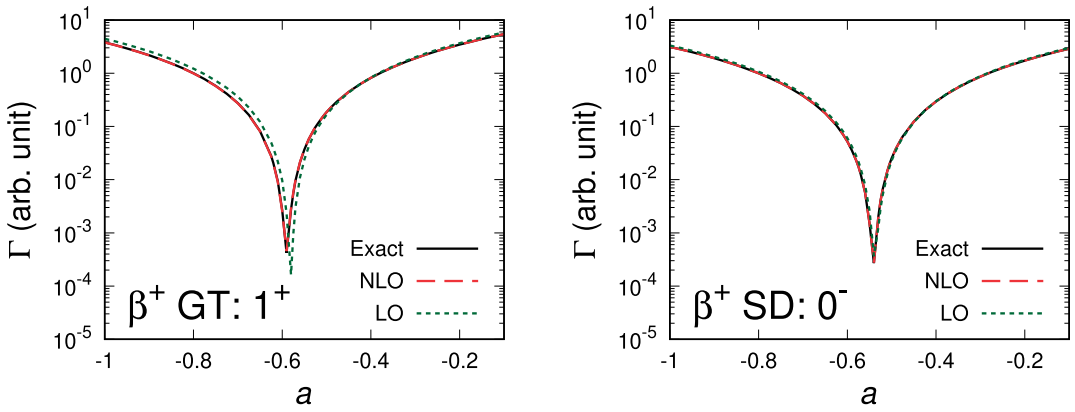

Fig. 6. Same as Fig. 5 but for β^+ decay.

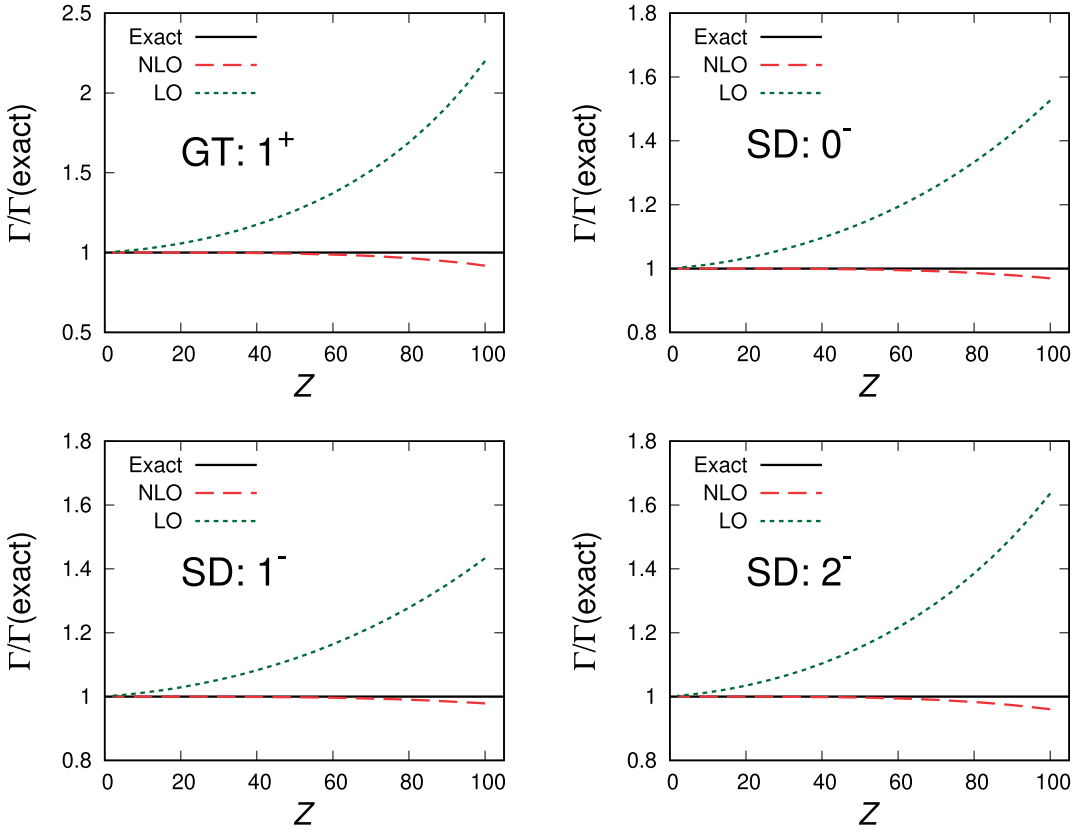

Fig. 7. Ratio of the β^- decay rate, $\Gamma(\mathrm{NLO})/\Gamma(\mathrm{exact})$ and $\Gamma(\mathrm{LO})/\Gamma(\mathrm{exact})$ for the GT $\Delta J^\pi = 1^+$, and the SD $\Delta J^\pi = 0^-$, 1^- and 2^- transitions. The decay rate is calculated for $E_0 = 10$ MeV, $A = 2Z$ and $a = -0.8$.

6. EDF transition density and NLO electron wave function

To investigate the validity of our formalism in realistic cases, we use the transition densities microscopically calculated by a nuclear energy-density functional (EDF) method. Since the details of the formalism can be found in Ref. [44], here we recapitulate the basic equations relevant to the present study. In the framework of the nuclear EDF method we employ, the ground state of a mother nucleus

is described by solving the Kohn–Sham–Bogoliubov (KSB) equation [45]

$$\begin{bmatrix} h^q(\boldsymbol{r}\sigma) - \lambda^q & \tilde{h}^q(\boldsymbol{r}\sigma) \\ \tilde{h}^q(\boldsymbol{r}\sigma) & -h^q(\boldsymbol{r}\sigma) + \lambda^q \end{bmatrix} \begin{bmatrix} \varphi^q_{1,\alpha}(\boldsymbol{r}\sigma) \\ \varphi^q_{2,\alpha}(\boldsymbol{r}\sigma) \end{bmatrix} = E_\alpha \begin{bmatrix} \varphi^q_{1,\alpha}(\boldsymbol{r}\sigma) \\ \varphi^q_{2,\alpha}(\boldsymbol{r}\sigma) \end{bmatrix}, \tag{82}$$

where the KS potentials h and $\tilde{h}$ are given by the EDF. An explicit expression of the potentials can be found, e.g. in the Appendix of Ref. [46]. The chemical potential λ is determined so as to give the desired nucleon number as an average value. The superscript q denotes n (neutron, $\tau_z = 1$) or p (proton, $\tau_z = -1$).

The excited states $|f;J^\pi\rangle$ in a daughter nucleus are described as one-phonon excitations built on the ground state $|i\rangle$ of the mother nucleus as

$$|f;J^\pi\rangle = \Gamma^\dagger_f |i\rangle, \tag{83}$$

$$\Gamma^\dagger_f = \sum_{\alpha\beta} \left\{ X^f_{\alpha\beta} a^\dagger_{\alpha,\mathrm{n}} a^\dagger_{\beta,\mathrm{p}} - Y^f_{\alpha\beta} a_{\beta,\mathrm{p}} a_{\alpha,\mathrm{n}} \right\}, \tag{84}$$

where $a^\dagger_\mathrm{n}(a^\dagger_\mathrm{p})$ and $a_\mathrm{n}(a_\mathrm{p})$ are the neutron (proton) quasiparticle (labeled by α and β) creation and annihilation operators that are defined in terms of the solutions of the KSB equation (82) with the Bogoliubov transformation. The phonon states, the amplitudes X^f, Y^f, and the vibrational frequency ω_f are obtained in the proton–neutron quasiparticle-random-phase approximation (pnQRPA). The residual interactions entering into the pnQRPA equation are given self-consistently by the EDF. With the solutions of the pnQRPA equation, the transition density is given as

$$g_A \delta\boldsymbol{\rho}_{f;J^\pi}(\boldsymbol{r}) = \langle f;J^\pi|\boldsymbol{A}(\boldsymbol{r})|i\rangle = \langle i|[\Gamma_f, \boldsymbol{A}(\boldsymbol{r})]|i\rangle \tag{85}$$

in a standard quasi-boson approximation. One obtains the transition density in the radial coordinate as

$$\rho_{JLK}(r) = \int d\Omega_r [Y_L(\hat{r}) \otimes \delta\boldsymbol{\rho}(\boldsymbol{r})]_{JK}, \tag{86}$$

which is independent of K in the present case for spherical systems. Thus, the input transition density is obtained by $\rho_{JL}(r) = \sqrt{2J+1}\rho_{JL0}(r)$.

We apply our formula for the medium-heavy Ni and Sn isotopes. Since a considerable contribution of the first-forbidden transition is predicted in the Sn isotopes [30], we take ^{160}Sn as an example in the present study. Furthermore, an interplay between the allowed and first-forbidden transitions has been discussed around ^{78}Ni [47], and we thus take ^{80}Ni as a target of the present study as well and employ the same Skyrme and pairing EDF as in Ref. [47]. Within the pnQRPA, the maximum electron energy is given as $E_0 = B(Z+1,N-1) - B(Z,N) + (m_\mathrm{n} - m_\mathrm{p} - m_e) \simeq \lambda^\mathrm{n} - \lambda^\mathrm{p} - \omega + 0.78$ MeV for β^- decay [21].

The transition densities ρ_{JL} of the $J^\pi = 1^+$ ($E_0 = 12.1$ MeV) and 0^- (16.1 MeV) states in ^{160}Sn are shown in Fig. 8. Those states give the largest contribution to the transition rate for each J^π. One sees there are nodes, similarly to the transition densities of the schematic model. In such a case, the contribution around the nuclear surface $r \sim R_A$ is important.

Using the transition densities microscopically calculated by the EDF method, we evaluate the half-life of β^- decay of the allowed Gamow–Teller and the first-forbidden spin-dipole transitions of ^{80}Ni and ^{160}Sn. The β decay rates are calculated within the impulse approximation for the space component of the axial vector current only. Here we use the effective axial vector coupling constant

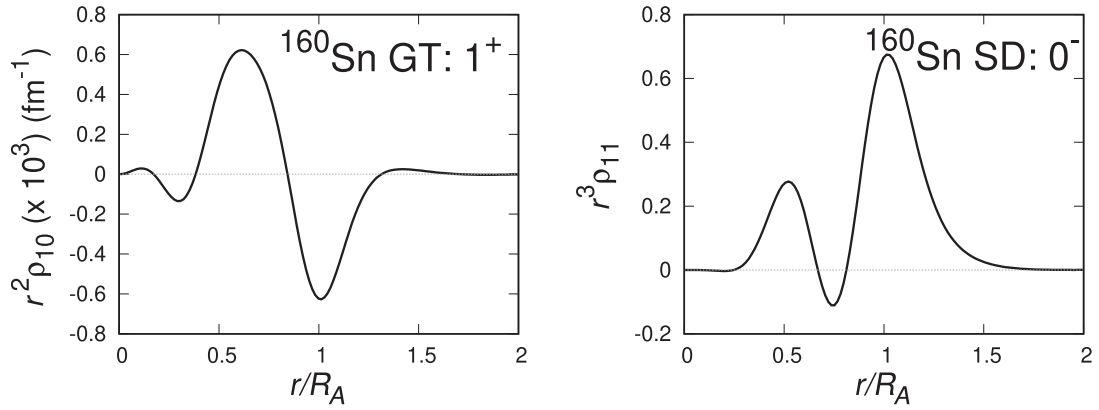

Fig. 8. Transition density $r^{2+L}\rho_{JL}$ of (left) GT transition $J^\pi = 0^+ \to 1^+$ ($E_0 = 12.1$ MeV) multiplied by 10^3 and (right) SD transition $J^\pi = 0^+ \to 0^-$ ($E_0 = 16.1$ MeV) of ^{160}Sn. The dotted horizontal line indicates zero.

Table 1. Half-life $t_{1/2}$ of the β^- decay of ^{80}Ni and ^{160}Sn to the daughter nucleus with the states J^π. The ratios of the half-life $t_{1/2}$ (LO)/$t_{1/2}$ (exact) and $t_{1/2}$ (NLO)/$t_{1/2}$ (exact) are denoted as LO and NLO, respectively.

J^π	^{80}Ni			^{160}Sn		
	$t_{1/2}$(s)	LO	NLO	$t_{1/2}$(s)	LO	NLO
1^+	3.50×10^{-1}	0.962	1.00	2.39×10^{-3}	0.874	1.00
0^-	1.08	0.928	1.00	1.34×10^{-2}	0.874	1.00
1^-	3.02	0.943	1.00	5.18×10^{-2}	0.895	1.00
2^-	2.18	0.942	1.00	1.42×10^{-1}	0.857	1.00

$g_A = 1$. The half-life is calculated using the "exact" formula without approximation for the lepton wave functions. The contribution of all the states up to $E_0 \sim 14$ MeV (16 MeV) for ^{80}Ni (^{160}Sn) are included. Shown in Table 1 is the half-life thus calculated for each J^π. We show the ratios of the half-life $t_{1/2}$(LO)/$t_{1/2}$ (exact) and $t_{1/2}$(NLO)/$t_{1/2}$ (exact) in the table as well. As suspected, the LO approximation overestimates the transition rate by about 5 to 15% depending on the type of the transition and nuclide. Therefore, the half-lives are underestimated. The deviation from the "exact" calculation is larger for Sn than for Ni. Introducing the NLO correction, those errors are nicely restored, as shown in the fourth and seventh columns of Table 1. We can therefore argue that our simple NLO formula is very effective in realistic calculations.

7. Summary

We have investigated the Coulomb effects on the beta-decay rate. The decay rate is determined by the product of the lepton and hadron current densities. A widely used formula relies on the fact that the low-energy lepton wave functions in a nucleus can be well approximated by a constant and are linear to the radius for the s-wave and p-wave wave functions, respectively. We found, however, that the Coulomb wave function is conspicuously different from such a simple approximation for heavy nuclei with large Z by numerically solving the Dirac equation. We then proposed formulas of the nuclear beta-decay rate that are useful in a practical calculation.

In our proposed formulas, the neutrino wave function is treated exactly as a plane wave, while the electron wave function is obtained by iteratively solving the integral equation; thus, we can control the uncertainty of the approximate electron wave function order by order. The leading-order

approximation gives a formula that is almost equivalent to the widely used one and overestimates the decay rate by about 50–100% for heavy nuclei with $Z \sim 80$. We demonstrated that the next-to-leading-order formula reproduces well the exact result for a schematic transition density as well as a microscopic one obtained by a nuclear energy-density functional method. For the beta decay involving heavy neutron-rich nuclei, the NLO will be needed for the determination of the Gamow–Teller strength from the beta-decay rate.

We considered only the space component of the axial vector currents and kept only the lowest multipoles. The time components as well as the vector currents can have a comparable contribution to the decay rate, and we plan to present these improvements in a sequel to the present article. The beta decay provides a unique spectroscopic tool of exotic nuclei, i.e. the angular correlation contains rich information of nuclear structure. Furthermore, the electron/muon capture is an important process in the application to astrophysics and fundamental physics. It is straightforward to extend our formalism in these directions.

Acknowledgements

We would like to thank Prof. K. Koshigiri for useful discussions. This work was in part supported by the Japan Society for the Promotion of Science (JSPS) KAKENHI Grants Nos. JP18H01210, JP18H04569, JP18K03635, JP19H05104, JP19H05140, and JP19K03824, the Collaborative Research Program 2019–2021, Information Initiative Center, Hokkaido University, and the JSPS/NRF/NSFC A3 Foresight Program "Nuclear Physics in the 21st Century." The nuclear EDF calculation was performed on CRAY XC40 at the Yukawa Institute for Theoretical Physics, Kyoto University.

Appendix A. Derivation of the decay rate

In this appendix, we show the derivation of the decay rate Eq. (16) for β^- decay. In the present case, it is useful to expand the effective Hamiltonian in terms of the angular momentum. With the partial wave expansion of the neutrino wave function, we get

$$(1-\gamma_5)\, v^{s_\nu}(p_\nu)\, e^{-i\boldsymbol{p}_\nu\cdot\boldsymbol{r}} = 4\pi \sum_{neu} \begin{pmatrix} -if_{\kappa_\nu}(r)\chi^{\mu_\nu}_{-\kappa_\nu} \\ g_{\kappa_\nu}(r)\chi^{\mu_\nu}_{\kappa_\nu} \end{pmatrix}, \tag{A.1}$$

where we use the abbreviated notation (upper sign) defined in Eq. (14). Since the neutrino mass is negligible, here we used $g_\kappa(r) = -S_\kappa f_{-\kappa}(r)$ and $f_\kappa(r) = S_\kappa g_{-\kappa}(r)$. We also have an alternative expression:

$$(1-\gamma_5)\, v^{s_\nu}(p_\nu)\, e^{-i\boldsymbol{p}_\nu\cdot\boldsymbol{r}} = 4\pi \sum_{neu} \begin{pmatrix} -g_{\kappa_\nu}(r)\chi^{\mu_\nu}_{-\kappa_\nu} \\ if_{\kappa_\nu}(r)\chi^{\mu_\nu}_{\kappa_\nu} \end{pmatrix}. \tag{A.2}$$

Thus, we obtain two equivalent expressions:

$$\begin{aligned} &\psi^{s_e(-)}_{p_e}(\boldsymbol{r})\,\gamma^\nu\,(1-\gamma_5)\, v^{s_\nu}(p_\nu)\, e^{-i\boldsymbol{p}_\nu\cdot\boldsymbol{r}} \\ &= (4\pi)^2 \sum_{el}\sum_{neu} \left(G_{\kappa_e}(r)\,\chi^{\mu_e\dagger}_{\kappa_e}, iF_{\kappa_e}(r)\,\chi^{\mu_e\dagger}_{-\kappa_e}(\hat{r}) \right) \gamma^\nu \begin{pmatrix} -if_{\kappa_\nu}(r)\chi^{\mu_\nu}_{-\kappa_\nu} \\ g_{\kappa_\nu}(r)\chi^{\mu_\nu}_{\kappa_\nu} \end{pmatrix} \qquad \text{(A.3)} \\ &= (4\pi)^2 \sum_{el}\sum_{neu} \left(G_{\kappa_e}(r)\,\chi^{\mu_e\dagger}_{\kappa_e}, iF_{\kappa_e}(r)\,\chi^{\mu_e\dagger}_{-\kappa_e}(\hat{r}) \right) \gamma^\nu \begin{pmatrix} -g_{\kappa_\nu}(r)\chi^{\mu_\nu}_{-\kappa_\nu} \\ if_{\kappa_\nu}(r)\chi^{\mu_\nu}_{\kappa_\nu} \end{pmatrix}, \qquad \text{(A.4)} \end{aligned}$$

where we used Eq. (13).

As in Eq. (2), the hadron current is composed of the vector and axial vector components. We can thus write

$$\begin{aligned}
&\psi_{p_e}^{s_e(-)}(\boldsymbol{r})\,\gamma^{\nu}\,(1-\gamma_5)\,v^{s_\nu}(p_\nu)\,e^{-i\boldsymbol{p}_\nu\cdot\boldsymbol{r}}J_\nu \\
&=(4\pi)^2\sum_{el}\sum_{neu}\left(G_{\kappa_e}(r)\,\chi_{\kappa_e}^{\mu_e\dagger}(\hat{r}),\,iF_{\kappa_e}(r)\,\chi_{-\kappa_e}^{\mu_e\dagger}(\hat{r})\right) \\
&\quad\times\left\{\left(\gamma^0V_0-\boldsymbol{\gamma}\cdot\boldsymbol{V}\right)\begin{pmatrix}-g_{\kappa_\nu}(r)\chi_{\kappa_\nu}^{\mu_\nu}(\hat{r})\\ if_{\kappa_\nu}(r)\chi_{-\kappa_\nu}^{\mu_\nu}(\hat{r})\end{pmatrix}-\left(\gamma^0A_0-\boldsymbol{\gamma}\cdot\boldsymbol{A}\right)\begin{pmatrix}-if_{\kappa_\nu}(r)\chi_{-\kappa_\nu}^{\mu_\nu}\\ g_{\kappa_\nu}(r)\chi_{\kappa_\nu}^{\mu_\nu}\end{pmatrix}\right\}. \qquad \text{(A.5)}
\end{aligned}$$

The products of the two-component spinors are given as

$$\chi_{\kappa}^{\mu\dagger}(\hat{r})\,\chi_{\kappa'}^{\mu'}(\hat{r})=\frac{1}{\sqrt{4\pi}}\sum_{L,M}\left(j_\kappa,-\mu,j_{\kappa'},\mu'|L,M\right)(-1)^{1/2-\mu}S_\kappa S_{0LL}(\kappa,\kappa')Y_{LM}(\hat{r}), \qquad \text{(A.6)}$$

$$\chi_{\kappa}^{\mu\dagger}(\hat{r})\,\sigma^i\chi_{\kappa'}^{\mu'}(\hat{r})=\frac{-1}{\sqrt{4\pi}}\sum_{J,L,M}\left(j_\kappa,-\mu,j_{\kappa'},\mu'|J,M\right)(-1)^{1/2-\mu}S_\kappa S_{1LJ}(\kappa,\kappa')\left[Y_L(\hat{r})\otimes(\epsilon^i)\right]_{JM}, \qquad \text{(A.7)}$$

where ϵ is a unit vector. Using these relations, we obtain the effective Hamiltonian Eqs. (11) and (12). According to the Wigner–Eckart theorem, the M-dependence of the spherical tensor Ξ_{JLM}, Eq. (12), is known as

$$\langle f|\,\Xi_{JLM}(\kappa_e,\kappa_\nu)\,|i\rangle=\frac{\left(J_i,s_i,J,M|J_f,s_f\right)}{\sqrt{2J_f+1}}\,\langle f||\,\Xi_{JL}(\kappa_e,\kappa_\nu)\,||i\rangle, \qquad \text{(A.8)}$$

where the reduced matrix element $\langle f||\,\Xi_{JL}(\kappa_e,\kappa_\nu)\,||i\rangle$ is independent of M, and J_f is the angular momentum of the final nuclear state.

With the obtained Hamiltonian $H_{\rm eff}$, the decay rate is given by

$$\begin{aligned}
\Gamma&=\frac{1}{2J_i+1}\sum_{s_i}\sum_{s_f,s_e,s_\nu}\int\frac{d^3p_\nu}{(2\pi)^3}\frac{d^3p_e}{(2\pi)^3}(2\pi)\delta(E_\nu+E_e-E_0)\,|H_{\rm eff}|^2 \\
&=\frac{G_F^2V_{ud}^2(4\pi)^3}{4(2\pi)^5}\int_{m_e}^{E_0}dE_ep_eE_e(E_0-E_e)^2\,\frac{1}{(2J_i+1)(2J_f+1)}\sum_{s_f,s_i}\sum_{s_e,s_\nu}\int d\Omega_ed\Omega_\nu \\
&\quad\times\left|\sum_{el}\sum_{neu}\sum_{J,L,M}(-1)^{1/2-\mu_e}\left(j_{\kappa_e},-\mu_e,j_{\kappa_\nu},\mu_\nu|J,M\right)\left(J_i,s_i,J,M|J_f,s_f\right)\langle f||\,\Xi_{JL}(\kappa_e,\kappa_\nu)\,||i\rangle\right|^2, \qquad \text{(A.9)}
\end{aligned}$$

where J_i is the angular momentum of the initial nuclear state. For an arbitrary function $X(\kappa,\mu)$, we have

$$\int d\Omega_e\sum_{s_e}\left|\sum_{el}X(\kappa_e,\mu_e)\right|^2=\sum_{\kappa_e,\mu_e}|X(\kappa_e,\mu_e)|^2, \qquad \text{(A.10)}$$

and

$$\int d\Omega_\nu\sum_{s_\nu}\left|\sum_{neu}X(\kappa_\nu,\mu_\nu)\right|^2=2\sum_{\kappa_\nu,\mu_\nu}|X(\kappa_\nu,\mu_\nu)|^2. \qquad \text{(A.11)}$$

Applying Eqs. (A.10) and (A.11), and the orthonormal relation of the Clebsh–Gordan coefficients to Eq. (A.9), one can perform all the angular integral and summation. We then arrive at Eq. (16).

Appendix B. Explicit formula for the uniform charge distribution

For the uniform charge distribution of nuclei with radius R_A, the Coulomb potential for an electron is given as

$$V_C(r) = -\frac{\alpha Z}{2R_A}\left[\theta(1-x)(3-x^2) + \theta(x-1)\frac{2}{x}\right], \tag{B.1}$$

where α is the fine structure constant and $x = r/R_A$. The electron wave functions $D^{(i)}, d^{(i)}, H^{(2)}$, and $h^{(2)}$ are given as

$$\frac{r}{R}D_k^{(1)}(r) = r\left[\frac{E_e}{2k+1} + \xi s_1(x)\right], \tag{B.2}$$

$$\frac{r}{R}d_k^{(1)}(r) = r\left[\frac{m_e}{2k+1}\right], \tag{B.3}$$

$$H^{(2)}(r) = r^2\left[-\frac{p_e^2}{2(2k+1)} + E_e\xi s_2(x) + \xi^2 t_2(x)\right], \tag{B.4}$$

$$h^{(2)}(r) = r^2[m_e\xi w_2(x)], \tag{B.5}$$

$$\frac{r}{R}D_k^{(3)}(r) = r^3\left[-\frac{p_e^2E_e}{2(2k+1)(2k+3)} + p_e^2\xi s_3(x) + m_e^2\xi t_3(x) + E_e\xi^2 w_3(x) + \xi^3 y_3(x)\right], \tag{B.6}$$

$$\frac{r}{R}d_k^{(3)}(r) = r^3\left[-\frac{p_e^2m_e}{2(2k+1)(2k+3)} + m_eE_e\xi t_3(x) + m_e\xi^2 z_3(x)\right], \tag{B.7}$$

where $\xi = \alpha Z/(2R_A)$ for an electron and $\xi = -\alpha Z/(2R_A)$ for a positron.

The functions s_a, t_a, w_a, y_a, and z_a for $k = 1$ are given as

$$s_1(x) = \theta(1-x)\left(1 - \frac{x^2}{5}\right) + \theta(x-1)\frac{1}{x}\left(1 - \frac{1}{5x^2}\right), \tag{B.8}$$

$$s_2(x) = \theta(1-x)\left(-1 + \frac{2x^2}{15}\right) + \theta(x-1)\frac{1}{x}\left(-\frac{5}{3} + \frac{1}{x} - \frac{1}{5x^2}\right), \tag{B.9}$$

$$t_2(x) = \theta(1-x)\left(-\frac{3}{2} + \frac{2x^2}{5} - \frac{x^4}{30}\right) + \theta(x-1)\frac{1}{x^2}\left(-\frac{14}{15} - \frac{1}{5x^2} - 2\ln x\right), \tag{B.10}$$

$$w_2(x) = \theta(1-x)\frac{x^2}{30} + \theta(x-1)\frac{1}{x}\left(\frac{1}{3} - \frac{1}{2x} + \frac{1}{5x^2}\right), \tag{B.11}$$

$$s_3(x) = \theta(1-x)\left(-\frac{3}{10} + \frac{3x^2}{70}\right) + \theta(x-1)\frac{1}{x}\left(-\frac{1}{2} + \frac{1}{3x} - \frac{1}{10x^2} + \frac{1}{105x^4}\right), \tag{B.12}$$

$$t_3(x) = \theta(1-x)\left(-\frac{1}{5}+\frac{x^2}{42}\right)+\theta(x-1)\frac{1}{x}\left(-\frac{1}{3}+\frac{1}{6x}-\frac{1}{105x^4}\right), \tag{B.13}$$

$$w_3(x) = \theta(1-x)\left(-\frac{9}{10}+\frac{9x^2}{35}-\frac{x^4}{54}\right) + \theta(x-1)\frac{1}{x^2}\left(-\frac{6}{5}+\frac{1}{x}-\frac{3}{5x^2}+\frac{131}{945x^3}-\frac{2\ln x}{3}\right), \tag{B.14}$$

$$y_3(x) = \theta(1-x)\left(-\frac{9}{10}+\frac{27x^2}{70}-\frac{x^4}{18}+\frac{x^6}{330}\right) + \theta(x-1)\frac{1}{x^3}\left(\frac{1}{15}-\frac{439}{693x^2}-2\ln x-\frac{2\ln x}{5x^2}\right), \tag{B.15}$$

$$z_3(x) = \theta(1-x)\left(-\frac{3}{10}+\frac{x^2}{14}-\frac{x^4}{135}\right) + \theta(x-1)\frac{1}{x^2}\left(\frac{2}{15}-\frac{1}{2x}+\frac{1}{5x^2}-\frac{131}{1890x^3}-\frac{2\ln x}{3}\right). \tag{B.16}$$

Similar formulas for $k = 2$ are given as

$$s_1(x) = \theta(1-x)\left(\frac{3}{5}-\frac{x^2}{7}\right)+\theta(x-1)\frac{1}{x}\left(\frac{1}{2}-\frac{3}{70x^4}\right), \tag{B.17}$$

$$s_2(x) = \theta(1-x)\left(-\frac{3}{5}+\frac{3x^2}{35}\right)+\theta(x-1)\frac{1}{x}\left(-\frac{9}{10}+\frac{2}{5x}-\frac{1}{70x^4}\right), \tag{B.18}$$

$$t_2(x) = \theta(1-x)\left(-\frac{9}{10}+\frac{9x^2}{35}-\frac{x^4}{42}\right)+\theta(x-1)\frac{1}{x^2}\left(-\frac{271}{420}-\frac{3}{140x^4}-\ln x\right), \tag{B.19}$$

$$w_2(x) = \theta(1-x)\frac{x^2}{70}+\theta(x-1)\frac{1}{x}\left(\frac{1}{10}-\frac{1}{10x}+\frac{1}{70x^4}\right), \tag{B.20}$$

$$s_3(x) = \theta(1-x)\left(-\frac{9}{70}+\frac{13x^2}{630}\right)+\theta(x-1)\frac{1}{x}\left(-\frac{11}{60}+\frac{2}{25x}-\frac{1}{140x^4}+\frac{4}{1575x^6}\right), \tag{B.21}$$

$$t_3(x) = \theta(1-x)\left(-\frac{3}{35}+\frac{x^2}{90}\right)+\theta(x-1)\frac{1}{x}\left(-\frac{2}{15}+\frac{3}{50x}-\frac{2}{1575x^6}\right), \tag{B.22}$$

$$w_3(x) = \theta(1-x)\left(-\frac{27}{70}+\frac{13x^2}{105}-\frac{23x^4}{2310}\right) + \theta(x-1)\frac{1}{x^2}\left(-\frac{943}{2100}+\frac{1}{5x}-\frac{1}{20x^4}+\frac{157}{5775x^5}-\frac{\ln x}{5}\right), \tag{B.23}$$

$$y_3(x) = \theta(1-x)\left(-\frac{27}{70}+\frac{13x^2}{70}-\frac{23x^4}{770}+\frac{x^6}{546}\right) + \theta(x-1)\frac{1}{x^3}\left(-\frac{83}{420}-\frac{87}{2860x^4}-\frac{\ln x}{2}-\frac{3\ln x}{70x^4}\right), \tag{B.24}$$

Table C1. Coefficients in Eq. (59) for the Gamow–Teller transition ($L = 0, \Delta J^\pi = 1^+$).

(κ_e, κ_ν)	(c_g, c_f)	(κ_e, κ_ν)	(c_g, c_f)
$(-1,-1)$	$(\sqrt{2}, \sqrt{2}/3)$	$(-2,1)$	$(4/3, 0)$
$(1,1)$	$(-\sqrt{2}/3, -\sqrt{2})$	$(2,-1)$	$(0, -4/3)$
$(-2,-2)$	$(-2\sqrt{5}/3, -2/\sqrt{5})$	$(1,-2)$	$(4/3, 0)$
$(2,2)$	$(2/\sqrt{5}, 2\sqrt{5}/3)$	$(-1,2)$	$(0, -4/3)$

Table C2. Same as Table C1 but for the spin-dipole transition ($L = 1, \Delta J^\pi = 0^-, 1^-, 2^-$).

	$J=0$	$J=1$	$J=2$
(κ_e, κ_ν)	(c_g, c_f)	(c_g, c_f)	(c_g, c_f)
$(-1,1)$	$(-\sqrt{2}, \sqrt{2})$	$(2/\sqrt{3}, 2/\sqrt{3})$	
$(1,-1)$	$(-\sqrt{2}, \sqrt{2})$	$(-2/\sqrt{3}, -2/\sqrt{3})$	
$(-2,2)$	$(2,-2)$	$(-4\sqrt{2/15}, -4\sqrt{2/15})$	$(\sqrt{2}/5, -\sqrt{2}/5)$
$(2,-2)$	$(2,-2)$	$(4\sqrt{2/15}, 4\sqrt{2/15})$	$(\sqrt{2}/5, -\sqrt{2}/5)$
$(-2,-1)$		$(\sqrt{2/3}, \sqrt{2/3})$	$(\sqrt{2}, \sqrt{2}/5)$
$(2,1)$		$(-\sqrt{2/3}, -\sqrt{2/3})$	$(-\sqrt{2}/5, -\sqrt{2})$
$(-1,-2)$		$(-\sqrt{2/3}, -\sqrt{2/3})$	$(\sqrt{2}, \sqrt{2}/5)$
$(1,2)$		$(\sqrt{2/3}, \sqrt{2/3})$	$(-\sqrt{2}/5, -\sqrt{2})$

$$z_3(x) = \theta(1-x)\left(-\frac{9}{70} + \frac{x^2}{30} - \frac{4x^4}{1155}\right) + \theta(x-1)\frac{1}{x^2}\left(-\frac{103}{2100} - \frac{1}{20x} + \frac{1}{140x^4} - \frac{157}{23100x^5} - \frac{\ln x}{5}\right). \tag{B.25}$$

Appendix C. Table of the coefficients in Ξ_{JLM}

For the axial vector space component, the effective operator is expressed as Eq. (59):

$$\Xi_{JLM}(\kappa_e, \kappa_\nu) = \int d\boldsymbol{r}[Y_L(\hat{r}) \otimes \boldsymbol{A}(\boldsymbol{r})]_{JM}[c_g G_{\kappa_e}(r) g_{\kappa_\nu}(r) + c_f F_{\kappa_e}(r) f_{\kappa_\nu}(r)].$$

Tables C1 and C2 list the explicit numbers of the coefficients of each (κ_e, κ_ν) for the Gamow–Teller and spin-dipole transitions, respectively.

Appendix D. Tables of electron and positron wave functions

We provide numerical tables of the four constants $\alpha_1, \alpha_{-1}, \alpha_2$, and α_{-2} needed to construct the electron and positron wave functions in this paper. Since these constants are strongly dependent on the electron momentum p_e and charge number Z of a nucleus, we rewrite them to L_0, λ_2, μ_1, and μ_2 according to Ref. [12]:

$$F(Z, E_e) = \alpha_{-1}^2 + \alpha_1^2 = F_0 L_0, \tag{D.1}$$

$$\lambda_2 = \frac{\alpha_{-2}^2 + \alpha_2^2}{\alpha_{-1}^2 + \alpha_1^2}, \tag{D.2}$$

$$\mu_k = \frac{kE_e}{\gamma_k m_e} \frac{\alpha_{-k}^2 - \alpha_k^2}{\alpha_{-k}^2 + \alpha_k^2}, \tag{D.3}$$

where

$$F_0(Z,E) = 4(2p_e R_A)^{-2(1-\gamma_1)} e^{\pi\nu} \left| \frac{\Gamma(\gamma_1 + i\nu)}{\Gamma(2\gamma_1+1)} \right|^2, \tag{D.4}$$

$$\gamma_k = \sqrt{k^2 - (\alpha Z)^2}, \tag{D.5}$$

$$\nu = \frac{\alpha Z E_e}{p_e}, \tag{D.6}$$

for the uniform nuclear charge distribution with radius R_A. In fact, these variables have a milder momentum and charge dependence than $\alpha_{\pm 1,2}$. First, we calculate $\alpha_{\pm 1,2}$ by numerically solving the Dirac equation and convert them into L_0, λ_2, μ_1, and μ_2 at various p_e/m_e and Z. These generated tables are respectively interpolated by assuming the following polynomial function at three regions, p_e/m_e =0.01–1, 1–10, and 10–100:

$$P(p_e/m_e, Z) = \sum_{t=-m}^{n} \left[\sum_{s=-m}^{n} W_{st} \left(\frac{p_e}{m_e} \right)^s \right] Z^t. \tag{D.7}$$

The weights of the polynomial W_{st} are determined by the least-square method. Finally, we reconstruct $\alpha_{\pm 1,2}$ from L_0, λ_2, μ_1, and μ_2. Since all $\alpha_{\pm 1,2}$ values are positive, the reconstruction can be made easily. We confirm that the resulting numerical tables are accurate to more than 3–4 digits with $(m,n) = (3,4)$.

For the convenience of a user, we provide a FORTRAN program code to generate $\alpha_{\pm 1,2}$ with a given p_e/m_e(=0.01–100) and Z(= 1–90) for $\beta^{\mp}$ decay as supplemental material [48]. The nuclear charge radius R_A is set to be $1.2A^{1/3}$ fm with the nuclear mass number A. To cover stable and neutron-rich unstable nuclei for the β^- decay, a variation of the charge radius can be considered among five options: $A = 2Z, 2.5Z, 3Z, 3.5Z$, and $4Z$.

References

[1] K. Langanke and G. Martínez-Pinedo, Rev. Mod. Phys. **75**, 819 (2003) [arXiv:nucl-th/0203071] [Search INSPIRE].
[2] B. P. Abbott et al. [LIGO Scientific and Virgo Collaborations], Phys. Rev. Lett. **119**, 161101 (2017) [arXiv:1710.05832 [gr-qc]] [Search INSPIRE].
[3] B. P. Abbott et al., Astrophys. J. Lett. **848**, L12 (2017) [arXiv:1710.05833 [astro-ph.HE]] [Search INSPIRE].
[4] S. Ando, J. A. McGovern, and T. Sato, Phys. Lett. B **677**, 109 (2009) [arXiv:0902.1194 [nucl-th]] [Search INSPIRE].
[5] A. Glick-Magid, Y. Mishnayot, I. Mukul, M. Hass, S. Vaintraub, G. Ron, and D. Gazit, Phys. Lett. B **767**, 285 (2017) [arXiv:1609.03268 [nucl-ex]] [Search INSPIRE].
[6] M. González-Alonso, O. Naviliat-Cuncic, and N. Severijns, Prog. Part. Nucl. Phys. **104**, 165 (2019) [arXiv:1803.08732 [hep-ph]] [Search INSPIRE].
[7] V. Cirigliano, A. Garcia, D. Gazit, O. Naviliat-Cuncic, G. Savard, and A. Young, arXiv:1907.02164 [nucl-ex] [Search INSPIRE].
[8] B. Stech and L. Schülke, Z. Phys. **179**, 314 (1964).
[9] L. Schülke, Z. Phys. **179**, 331 (1964).
[10] H. Behrens and W. Bühring, Nucl. Phys. A **162**, 111 (1971).
[11] H. F. Schopper, *Weak Interactions and Nuclear Beta Decay*, (North-Holland Publishing Company, Amsterdam, pp. 272–277, 1966).

[12] H. Behrens and J. Jänecke, *Numerical Tables for Beta-Decay and Electron Capture*, (Springer-Verlag, Berlin/Heidelberg, 1969).
[13] M. Morita, Prog. Theor. Phys. Suppl. **26**, 1 (1963).
[14] M. Morita, *Beta decay and muon capture* (W. A. Benjamin, Inc., Massachusetts, 1973).
[15] K. Koshigiri, M. Nishimura, H. Ohtsubo, and M. Morita, Nucl. Phys. A **319**, 301 (1979); **340**, 482 (1980) [erratum].
[16] W. Bühring, Nucl. Phys. **40**, 472 (1963).
[17] M. E. Rose, Phys. Rev. **82**, 389 (1951).
[18] N. B. Gove and M. J. Martin, At. Data Nucl. Data Tab. **10**, 205 (1971).
[19] E. K Warburton, J. A Becker, B. A. Brown, and D. J. Millener, Ann. Phys. **187**, 471 (1988).
[20] E. K. Warburton, Phys. Rev. C **44**, 233 (1991).
[21] J. Engel, M. Bender, J. Dobaczewski, W. Nazarewicz, and R. Surman, Phys. Rev. C **60**, 014302 (1999) [arXiv:nucl-th/9902059] [Search INSPIRE].
[22] P. Möller, B. Pfeiffer, and K.-L. Kratz, Phys. Rev. C **67**, 055802 (2003).
[23] I. N. Borzov and S. Goriely, Phys. Rev. C **62**, 035501 (2000).
[24] I. N. Borzov, Phys. Rev. C **67**, 025802 (2003).
[25] I. N. Borzov, Nucl. Phys. A **777**, 645 (2006).
[26] J. J. Cuenca-García, G. Martínez-Pinedo, K. Langanke, F. Nowacki, and I. N. Borzov, Eur. Phys. J. A. **34**, 99 (2007).
[27] T. Suzuki, T. Yoshida, T. Kajino, and T. Otsuka, Phys. Rev. C **85**, 015802 (2012) [arXiv:1110.3886 [nucl-th]] [Search INSPIRE].
[28] Z. M. Niu, Y. F. Niu, H. Z. Liang, W. H. Long, T. Nikšić, D. Vretenar, and J. Meng, Phys. Lett. B **723**, 172 (2013) [arXiv:1210.0680 [nucl-th]] [Search INSPIRE].
[29] Q. Zhi, E. Caurier, J. J. Cuenca-García, K. Langanke, G. Martínez-Pinedo, and K. Sieja, Phys. Rev. C **87**, 025803 (2013) [arXiv:1301.5225 [nucl-th]] [Search INSPIRE].
[30] M. T. Mustonen and J. Engel, Phys. Rev. C **93**, 014304 (2016) [arXiv:1510.02136 [nucl-th]] [Search INSPIRE].
[31] T. Marketin, L. Huther, and G. Martínez-Pinedo, Phys. Rev. C **93**, 025805 (2016) [arXiv:1507.07442 [nucl-th]] [Search INSPIRE].
[32] E. M. Ney, J. Engel, T. Li, and N. Schunck, Phys. Rev. C **102**, 034326 (2020) [arXiv:2005.12883 [nucl-th]] [Search INSPIRE].
[33] M. Morita and A. Fujii, Phys. Rev. **118**, 606 (1960).
[34] S. Nakamura, T. Sato, V. Gudkov, and K. Kubodera, Phys. Rev. C **63**, 034617 (2001); **73**, 049904 (2006) [erratum] [arXiv:nucl-th/0009012] [Search INSPIRE].
[35] J. D. Walecka, *Semileptonic weak interactions in nuclei in Muon physics II*, eds V. W. Hughes and C. S. Wu (Academic Press, Inc., New York, 1975).
[36] T. De Forest Jr. and J. D. Walecka, Adv. Phys. **15**, 1 (1966).
[37] S. X. Nakamura et al., Rept. Prog. Phys. **80**, 056301 (2017) [arXiv:1610.01464 [nucl-th]] [Search INSPIRE].
[38] L. Alvarez-Ruso et al., Prog. Part. Nucl. Phys. **100**, 1 (2018) [arXiv:1706.03621 [hep-ph]] [Search INSPIRE].
[39] K. Yoshida, Phys. Rev. C **96**, 051302(R) (2017) [arXiv:1709.10272 [nucl-th]] [Search INSPIRE].
[40] P. A. Zyla et al. [Particle Data Group], Prog. Theor. Exp. Phys. **2020**, 083C01 (2020).
[41] H. Feshbach and A. de Shalit, *Theoretical Nuclear Physics* (John Wiley & Sons, New York, 1974), Vol. 1.
[42] M. E. Rose, *Elementary theory of angular momentum* (John Wiley & Sons, New York, 1957).
[43] E. U. Condon and G. H. Shortley, *The theory of atomic spectra* (Cambridge University Press, Cambridge, 1935).
[44] K. Yoshida, Prog. Theor. Exp. Phys. **2013**, 113D02 (2013); **2021**, 019201 (2021) [erratum] [arXiv:1308.0424 [nucl-th]] [Search INSPIRE].
[45] J. Dobaczewski, H. Flocard, and J. Treiner, Nucl. Phys. A **422**, 103 (1984).
[46] H. Kasuya and K. Yoshida, Prog. Theor. Exp. Phys. **2021**, 013D01 (2021) [arXiv:2005.03276 [nucl-th]] [Search INSPIRE].
[47] K. Yoshida, Phys. Rev. C **100**, 024316 (2019) [arXiv:1903.03310 [nucl-th]] [Search INSPIRE].
[48] See Supplemental Material at http://... for the FORTRAN program code.